ARCHIVES OF ACOUSTICS
16, 3–4, 501–511 (1991)

USE OF ANTHROPOMORPHIC COMPRESSED BREAST PHANTOMS FOR COMPARING ULTRASOUND BREAST IMAGERS

E. KELLY-FRY

Indiana University School of Medicine Indianapolis, Indiana, USA

E. L. MADSEN, G. R. FRANK

University of Wisconsin, Madison, Wisconsin, USA

Two anthropomorphic breast phantoms were used to compare state-of the art ultrasound imagers. The phantoms mimic refractive effects at fat to nonfat boundaries, and include simulated and pathological structures like fibroadenomas, cysts, calcifications and malignant tumors. Images of those structures obtained by means of various ultrasound systems are compared and discussed. In conclusion, the authors recommend use anthropomorphic breast phantoms which simulate the acoustic characteristics of normal and pathological breast tissues to test ultrasound mammography systems prior to their routine use on patients.

Two anthropomorphic breast phantoms representing the compressed breast – and already reported in the literature [1] were used to compare state-of-the-art ultrasound imagers. The phantoms mimic the breast regarding attenuation and refractive effects at fat to nonfat boundaries. This includes bulk ultrasonic properties and geometric factors.

Diagrams of the contents of the first phantom (phantom I) are shown in Fig. 1. Three different views are shown. In Fig. 1 a is a view from the top. The phantom is 24 by 10 cm, as viewed, and includes 19 simulated spherical masses and one large fat-mimicking sphere. Of most importance in the present paper are six sets of 3 identical tissue-mimicking masses labeled *A B C E F* and *G*. For example, row *A* consists of 3 identical 6.3 mm diameter very highly attenuating spheres. These differ in their depth in the simulated glandular region. These three are also depicted in the side view shown in Fig. 1b. Their differences in depth are illustrated. Row *B* consists of 6.3 mm diameter low scatter masses representing fibroadenomas. Row *C* contains 6.3 mm diameter simulated cysts, Row *E*, 9.5 mm diameter cysts, Row *F*,

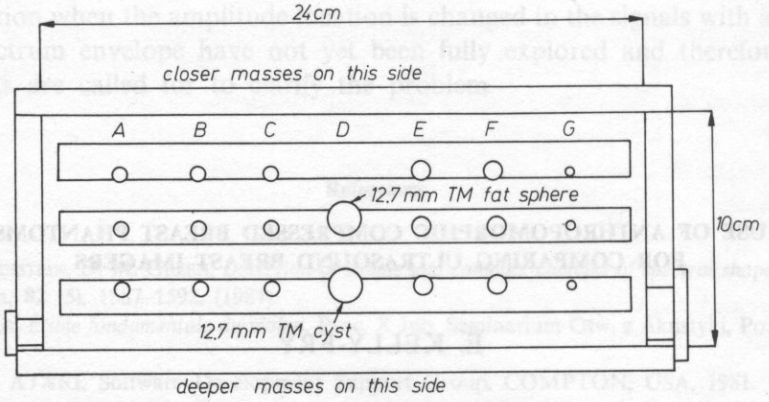

FIG. 1a. Diagram of phantom I viewed through the scanning window. Rows *A*, *B*, *C*, *E*, *F* and *G* each contain three identical spherical simulated lesions suspended in the tissue-mimicking *TM* glandular region. Row *D* contains two 12.7 mm diameter spherical objects, the upper one, a *TM* fat sphere and the lower one a *TM* cyst

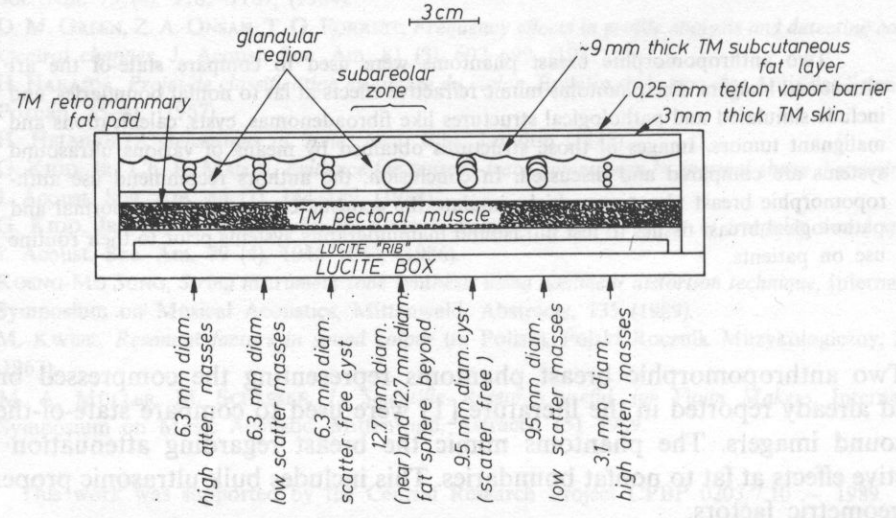

FIG. 1b. Side view diagram of phantom I showing the various layers of *TM* material and the different depths of the simulated lesions. An end view of the 1 mm diameter stacked agar rods simulating pectoral muscle bundles is shown. Also note the undulating interface between the *TM* subcutaneous fat layer and the glandular region

9.5 mm low scatter masses. Row *G* contains 3 mm diameter high attenuation masses composed of the same material as those in Row *A*. Notice the realistic irregularly shaped interface between the subcutaneous fat and the glandular region. Also of importance, regarding realistic beam distortions, is the fact that 25% of the

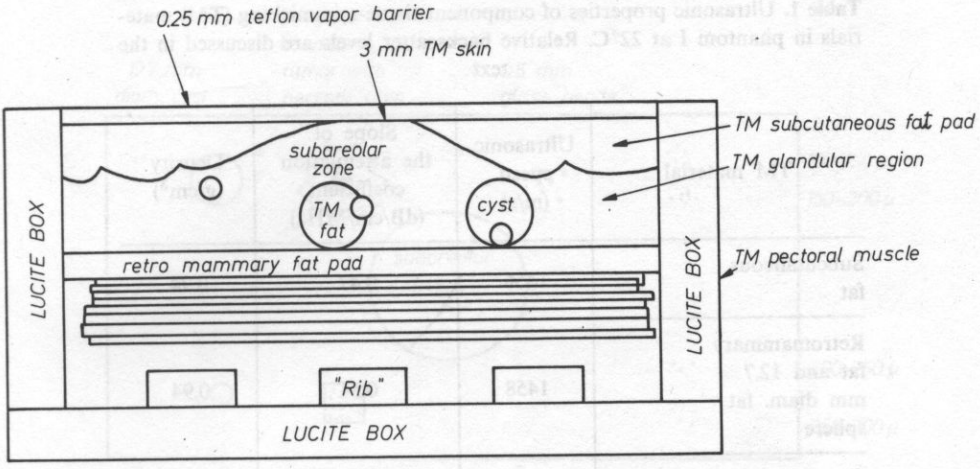

FIG. 1c. End view diagram of phantom I again showing the different depths of the lesions in the identical sets of three

glandular region is composed of randomly positioned fat spheres having diameters between 3 and 6 mm. In Fig. 1c is shown an end view of the phantom with the increasing depth of sets of three masses shown more plainly.

In Table 1 are shown ultrasonic properties of the contents of the phantom. Of importance is the much lower ultrasonic speed in the simulated fat, 1456 m/s, compared to that in the other simulated tissues. The fat also has a lower density, 0.94 gm/cm^3, compared to 1.03. Notice also the low attenuation in the cysts, 0.1 dB/cm/MHz, and the very high value of 8.7 dB/cm at 3 MHz for the highly attenuating spheres.

Fig. 2a and 2b depict phantom II, which is simpler in some ways than phantom I. Relatively large calcifications are represented with 4 one-half mm diameter glass beads. Smaller calcifications are represented with 5 sets of calcium hydroxyapatite particles varying from 100 through 300 microns in diameter. One set of 250 to 300 micron diameter particles are embedded in the glandular parenchyma, and another such set is embedded in an approximately 1 cubic cm volume having a backscatter level 6 dB below that of the surrounding glandular parenchyma. Notice also the simulated malignant tumor with a highly attenuating necrotic corea. A 4 mm diameter low scatter simulated fibroadenoma is also present. Another difference between this phantom and phantom I is that there are no fat spheres distributed in the glandular region.

The remaining figures emphasize the importance of breast phantoms in determining whether a specific imaging system can identify small masses located in **deep** regions of the breast and whether that system is also capable of definitively imaging the wall characteristics and internal structures of breast masses.

In Fig. 3a is an image obtained with the Siemens sonoline SL-1; that in Fig. 3b with the Aloka 620. All three of the three mm diameter highly attenuation masses in

Table 1. Ultrasonic properties of component tissue-mimmicking (TM) materials in phantom I at 22°C. Relative backscatter levels are discussed in the text

TM material	Ultrasonic speed (m/s)	Slope of the attenuation coefficient (dB/cm/MHz)	Density (g/cm^3)
Subcutaneous fat	1456	0.47	0.94
Retromammary fat and 12.7 mm diam. fat sphere	1458	0.54	0.94
Glandular parenchyma	1569	0.34	1.03
Fat spheres composing 25% of glandular region	1445	0.3	0.92
Cysts	1568	0.1	1.02
Low scatter lesions ("fibroadenomas")	1564	0.34	1.03
High attenuation lesions	1508	8.7 at 3 MHz	1.05
Pectoral muscle	1540	0.4	1.08
Skin	1570	0.6	1.05

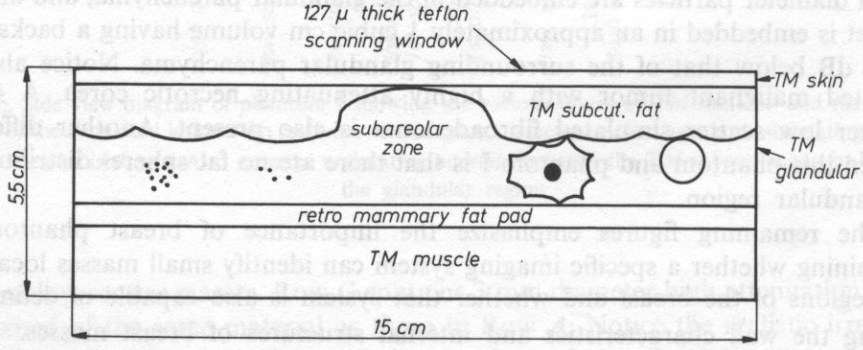

FIG. 2a. Side view diagram of the contents of phantom I including calcifications and a simulated malignancy with a necrotic core. The 8 cm × 15 cm scanning window is perpendicular to the figure.

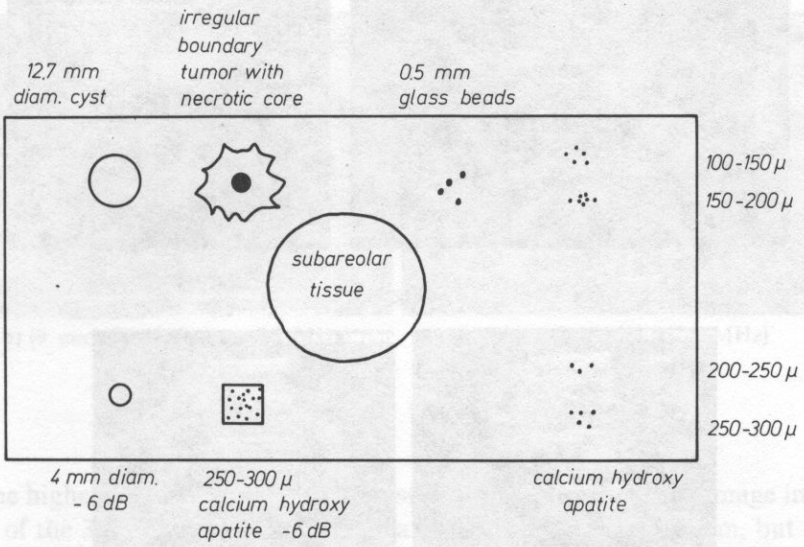

FIG. 2b. Diagrammatic view of anthropomorphic compressed breast phantom II from the scanning window side. Various objects are embedded in the *TM* glandular parenchyma. Six sets of simulated calcification are shown, five of which are Calcium hydroxyapatite, which is the inorganic component of bone. The leftmost set of calcifications are randomly suspended in a 0.5 cm^3 volume of *TM* abnormal tissue having a − 6 dB scatter level relative to the *TM* glandular parenchyma. Also shown is a realistic simulated tumor with an irregular boundary and a highly attenuating necrotic core. The vital part of the tumor is at − 6 dB scatter level relative to the glandular parenchyma except for two small "chips" of higher scatter material present to produce an irregular internal texture

phantom I are distinctly visible in Fig. 3a. In Fig. 3b, the mass closest to the surface is visible, and that located mid-region is also imaged. A significant finding was that the deepest mass could not be adequately imaged with this 7.5 MHz system.

Figures 4a and 4b show images of the 3 mm high attenuation mass closest to the phantom surface. That in Fig. 4a was obtained with the 6 MHz, linear array Phillips system and that in Fig. 4b with the 5 MHz linear array Acuson system. Note that

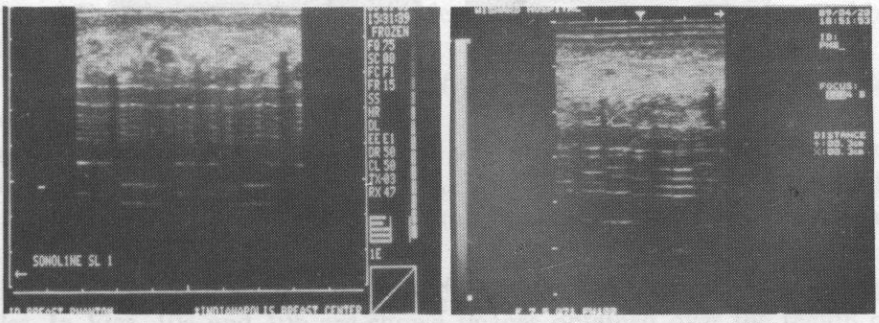

a) (Siemens − 7.5 MHz) b) (Aloka − 7.5 MHz)

Fig. 3. Images of 3 mm masses in Phantom I

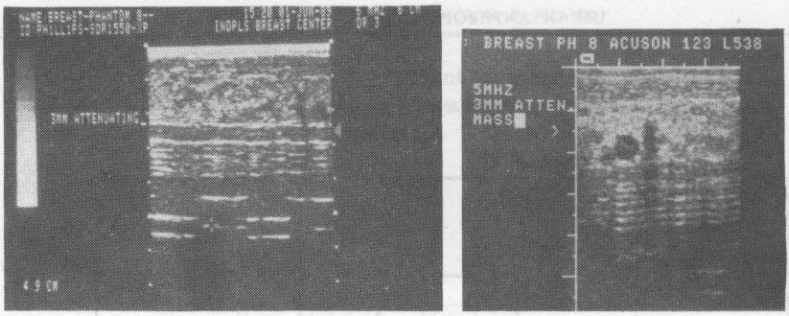

a) b)

Fig. 4

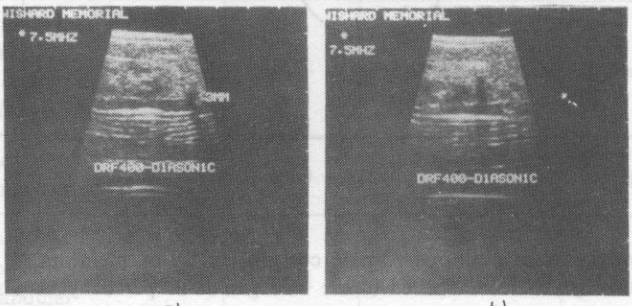

a) b)

Fig. 5

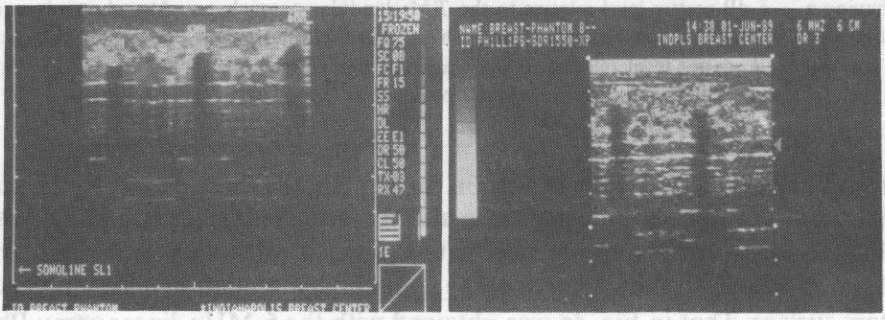

a) b)

Fig. 6

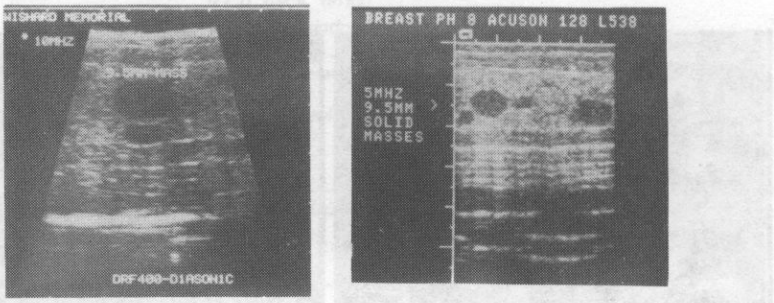

a) Fig. 7 b)

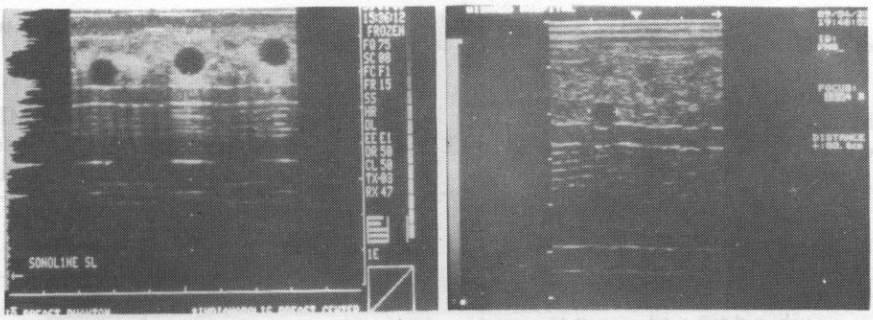

a) (9 mm Cysts-Siemens 7.5 MHz) *b)* (6 mm Cyst-Aloka 7.5 MHz)

Fig. 8

FIG. 3–8. Images of cystic structures in phantom I

despite the higher frequency, the 3 mm mass is poorly shown on the image in Fig. 4a. All three of the 3 mm masses could be located with the 5 MHz system, but only the most shallow one could be detected with the 6 MHz system, that is, the 6 MHz system could not locate either the mid-depth or deepest mass.

It was found that the Diasonics 7.5 MHz sector scanner was capable of imaging all three of these 3 mm masses. The deepest and most shallow are shown in Figs. 5a and 5b.

All of the tested systems could detect the 6 mm highly attenuating masses irrespective of the depth of their location. The Siemens 7.5 MHz linear array system provided the image in Fig. 6a, and the Phillips 6 MHz linear array system provided the image shown in Fig. 6b. Note the difference in resolution of wall structures in these two images.

Figures 7a and 7b are of interest because they compare images of the same solid mass by a 10 MHz sector scanner (Fig. 7a) and a 5 MHz linear array scanner (Fig. 7b). As you can see, in this case, the **lower** frequency system provided an image which is far superior to that of the higher frequency system.

All of the tested systems were capable of imaging all cysts shown in Phantom I. Figure 8a shows three 9.5 mm cysts imaged by the Siemens 7.5 MHz linear array system, and Fig. 8b shows an image of a deeply located 6 mm cyst as imaged by the 7.5 MHz linear array Aloka system.

The remaining figures show images of phantom II in the regions of simulated microcalcifications.

Images of the 1/2 mm glass beads are shown in Figs. 9a and 9b. The image in Fig. 9a was obtained with the 5 MHz Acuson system, that in Fig. 9b with the 5.0 MHz Aloka system. All of the systems tested were capable of imaging the highly reflective glass beads.

However, none could image the 100–300 micron calcium hydroxy apatite particles. In Figs. 10a and 10b are shown images obtained over the region of the 250–300 micron particles suspended in the 1 cm^3 low scatter tissue-mimicking

Table 2. Ultrasonic properties of TM materials in phantom II at 22°C: c ≡ ultrasonic speed; α/f ≡ slope of the attenuation coefficient with frequency; ϱ ≡ density; η ≡ backscatter coefficient

TM material	c (m/s)	α/f (dB/cm/MHz)	ϱ gm/ml	η (sr^{-1} cm^{-1})	η at 5 MHz relative to glandular (dB)
TM glandular	1561	0.36	1.04	$4.4X10^{-3}$ *	0
Subcutaneous fat	1458	0.43	0.94		−12
Retromammary fat	1458	0.40	0.94		−11
Tumor around necrotic core	1554	0.70	1.07		−6
Low scatter lesion with calcifications	1556	0.56	1.06		−6
Muscle	1559	0.55	1.05		+6
low scatter 4 mm mass	1561	0.33	1.04		−6
cyst	1560	0.12	1.02		--

* **in vivo** breast glandular tissue at 5 MHz: $\eta \sim 6X10^{-3}$ sr^{-1} cm^{-1} (DAVROS et al., 1986)

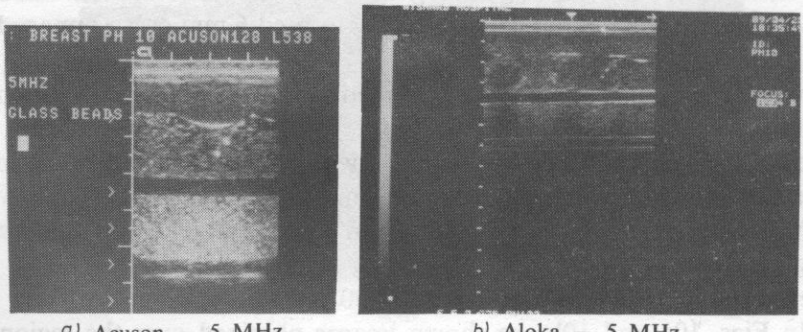

a) Acuson — 5 MHz b) Aloka — 5 MHz

Fig. 9. Images of 5 mm glass beads in phantom II

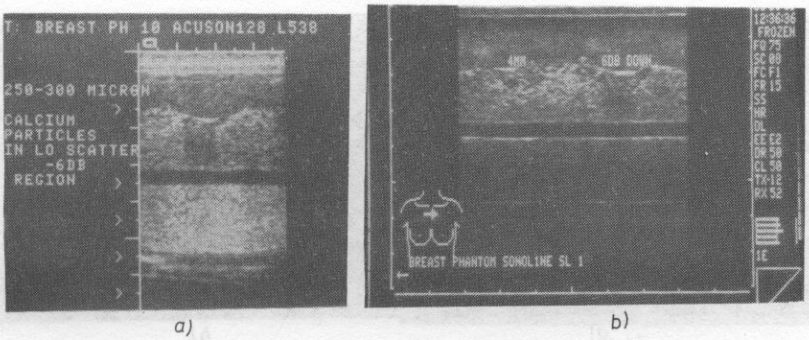

Fig. 10. Failure to image 100–300 micron particles in low-scatter region of Phantom II

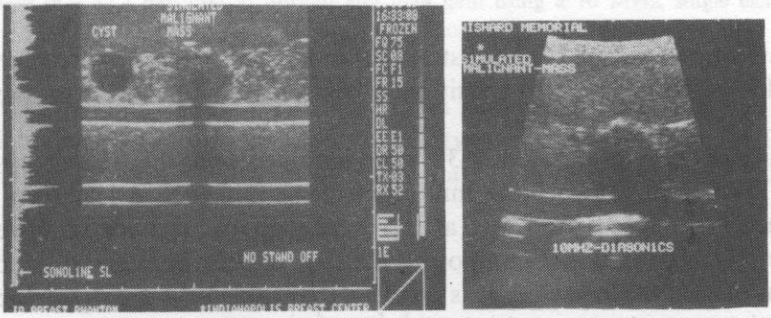

Fig. 11. Images of cept and simulated malignant mass at 7.5 MHz (a) and of same malignant at 10 MHz (b). Phantom II

region. Note in both images that the low-scatter – 6dB tissue mimicking region is recognizable, but no highly reflective particles are imaged within this region. In Fig. 10b, the 4 mm, low-scatter mass is also imaged. This small mass could be detected by all of the systems, but in some cases, it was not apparent whether this was a solid or cystic mass.

The simulated malignant mass was imaged by all of the real-time systems, but accurate delineation of its wall and internal structure was highly dependent on design of the ultrasound unit. Figure 11a shows an image of the malignant mass, and associated cyst, obtained with the 7.5 MHz Siemens system. Figure 11b shows this same mass as imaged with the Diasonics 10 MHz sector transducer. Both of these images include the region of the necrotic core. As you can see, the necrotic core is sharply imaged in Fig. 11a but is barely visible in Fig. 11b.

The images in Figs. 12a and 12b are still controversial regarding their meaning. They were made using an Aloka 7.5 MHz linear array and show a large cyst in a real breast. The cystic nature was verified by needle aspiration. In Fig. 12a the cyst is essentially echo free. In Fig. 12b, however – at a higher gain – artifactual echoes in the cyst are seen and a misdiagnosis of a solid mass could be made. Notice that the echoes have an irregular boundary. Presumably reverberations involving

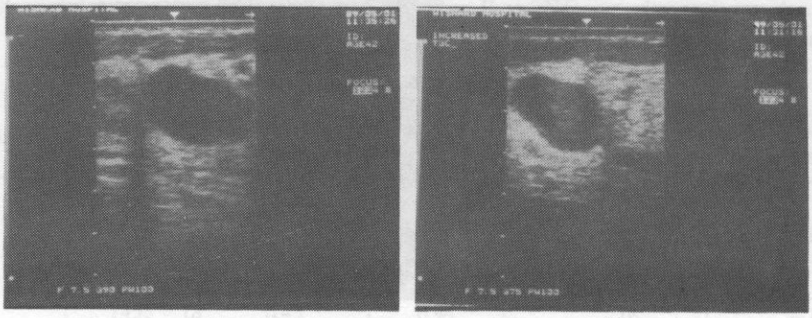

a) b)

FIG. 12. Images of a large cyst in a real breast

strong scatterers proximal to the cyst are involved, but perhaps these reverberations are added to strong laterially positioned scatterers to give rise to the irregular boundary.

The images in Figs. 13a and 13b were obtained with the Acuson system using phantom II. In Fig. 13a the 12.7 mm diameter simulated cyst is shown essentially free of echos. In Fig. 13b, however, at increased gain, discrete echoes have appeared within the cyst. The material composing the cyst is clear pure gelatin and therefore no internal echoes are expected. It is possible that these echoes are sidelobe artifacts related to the strong scatterers in the simulated glandular parenchyma lateral to the cyst. However, we have not yet ruled out the possibility that some imputities giving rise to echoes actually exist in the cyst.

Some evidence that the side-lobe explanation is the true one is offered in the images in Figs. 14a and 14b, obtained with a 10 MHz single element focused system. The cyst is imaged on the left in Fig. 14a at intermediate gain and in Fig. 14b at high gain. The cyst is echo free in both cases.

In summary, based on the variability of the systems tested with respect to their capability of detecting small deeply located masses and their ability to provide adequate image data on the structural characteristics of masses, the following recommendation is made.

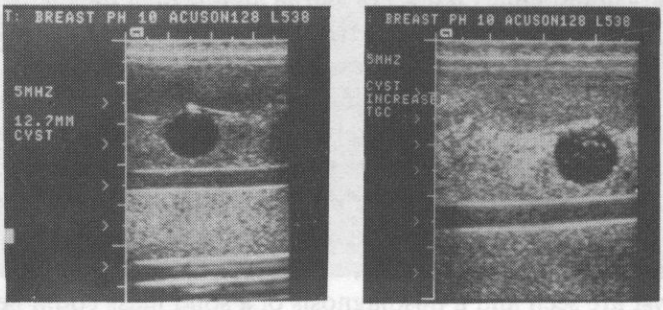

a) b)

Fig. 13. Images of a 12.7 mm cept at normal and high gain using a 5 MHz real-time system (Phantom II)

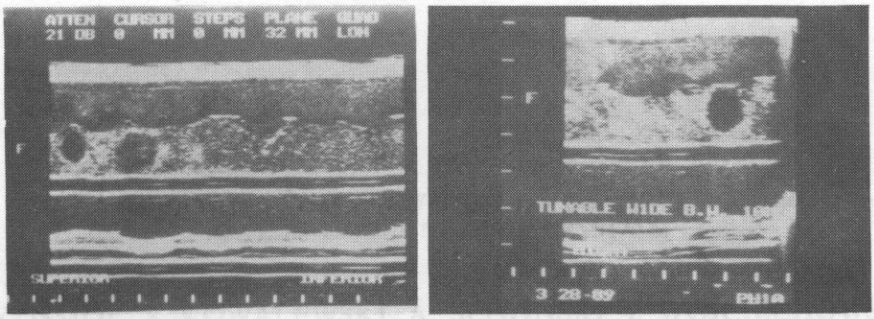

a) b)

Fig. 14. Images of a 12.7 mm cyst at normal and high gain using a 10 MHz, single element focused transducer. (Phantom II)

Anthropomorphic breast phantoms which simulate the acoustic characteristics of normal breast tissues and that of various type of benign and malignant breast masses should be used to test ultrasound mammography systems prior to their routine use on patients.

Acknowledgement

This work was supported in part by NIH grant RO1CA25634. Figures 1 and 2 and Tables 1 and 2 have been reproduced from Ref. [1] with permission of the publishers of Ultrasound in Med. and Biol.

References

[1] E. L. Madsen, E. Kelly-Fry, G. R. Frank, *Anthropomorphic phantoms for assessing systems used in ultrasound imaging of the compressed breast*, Ultrasound in Med. and Biol. **14**, Sup. 1, 183–201 (1988).

Received December 7, 1990